IEEE Access
Multidisciplinary | Rapid Review | Open Access Journal

Received October 22, 2021, accepted November 8, 2021, date of publication November 9, 2021,
date of current version November 19, 2021.

Digital Object Identifier 10.1109/ACCESS.2021.3126868

2D and 3D Visualizations of the Mass-Damper-Spring Model Dynamics Controlled by a Servo-Controlled Linear Actuator

ALI KANDIL[1], Y. S. HAMED[2], ABDULLAH M. ALSHARIF[2], AND JAN AWREJCEWICZ[3]
[1]Department of Physics and Engineering Mathematics, Faculty of Electronic Engineering, Menoufia University, Menouf 32952, Egypt
[2]Department of Mathematics and Statistics, College of Science, Taif University, Taif 21944, Saudi Arabia
[3]Department of Automation, Biomechanics and Mechatronics, Faculty of Mechanical Engineering, Lodz University of Technology, 90-924 Lodz, Poland

Corresponding author: Ali Kandil (alikandil21@el-eng.menofia.edu.eg)

This research was supported by Taif University Researchers Supporting Project Number (TURSP-2020/96), Taif University, Taif, Saudi Arabia. This research was also supported by the National Science Centre, Poland, under the Grant OPUS 14 No. 2017/27/B/ST8/01330.

ABSTRACT This paper focuses on controlling the dynamics of a mass-damper-spring model via a servo-controlled linear actuator (SCLA). The displacements of the mass are sensed and measured by a linear variable differential transformer (LVDT) whose output electrical signal is proportional with the position of the mass. Furthermore, a positive position feedback (PPF) controller is then provided with this signal to be processed and to generate the suitable control signal. The control signal itself is applied to the actuator which in turn controls the mass position. The whole system dynamical equations for the amplitudes and phases are derived with the aid of Krylov-Bogoliubov averaging perturbation method. 2D and 3D visualizations are included to give the reader a wider aspect of the system behavior before and after control.

INDEX TERMS Mass-damper-spring model, servo-controlled linear actuator, linear variable differential transformer, Krylov-Bogoliubov averaging perturbation method, positive position feedback controller.

I. INTRODUCTION

In mechanical engineering, there are various models that may suffer from unwanted vibrations, especially vehicles. The vehicles, including cars, have safety systems to eliminate or reduce the vibrations resulting from bumps which annoy the passengers. Many physicists have implemented such models in the form of a mass-damper-spring model and tried to control it. Ji and Zhang [1], [2] suppressed a forced nonlinear oscillator's vibrations via a mass-spring-damper absorber considering the primary and super-harmonic resonance cases. Alsaleem and Younis [3] have stabilized a DC-actuated and/or AC-actuated MEMS resonator by adopting a feedback controller with time-delay used originally in a pull-in frequency band. Febbo [4] utilized the harmonic balance method for extracting amplitude-phase-frequency equations that describe the harmonically driven oscillator's dynamical behavior. Ji *et al.* [5] explored the Hopf bifurcation's effect on a nonlinear oscillator's trivial equilibrium in case of increasing the time delay of the feedback controller.

The associate editor coordinating the review of this manuscript and approving it for publication was Qiuye Sun.

Liu *et al.* [6] investigated a harmonically-excited Euler-Bernoulli beam at primary and secondary resonances under the control of delayed-feedback. Bavastri *et al.* [7] designed an optimal viscoelastic vibration absorber which was coupled to a single degree-of-freedom (DOF) system. Beltrán-Carbajal *et al.* [8] extended a vibration absorber's capability as an absorption scheme for multi-excitation frequencies in order to perform a trajectory tracking for the main system. Ji [9] focused on the secondary resonance case of a time-delayed nonlinear oscillator via the center manifold theorem. Yang *et al.* [10] investigated a two DOF system's vibration characteristics for examining nonlinear absorbers' performance in suppressing primary oscillators' vibrations. Ji [11] explored the coexistence of bi-stable periodic solutions depending on the initial conditions of a time-delayed nonlinear oscillator on one condition of losing the trivial equilibrium's stability. Sun and Jing [12] subdued the 3D quasi-zero-stiffness property in a novel vibration isolator in order to symmetrize scissor-like structures in the horizontal and vertical directions along with a spring-mass-damper model. Febbo *et al.* [13] studied the effects of temperature change on two viscoelastic absorbers' design made of distinct materials.

Han and Cao [14] studied different types of bifurcations and limit cycles when adopting a nonlinear perturbation with a rotating pendulum model. El-Ganaini *et al.* [15] showed the time delay effects on PPF-controlling the vibrations of a magnetically-suspended mass subjected to a combination of force excitations. Shen *et al.* [16] designed an improved inerter vibration absorber coupled to the body of a vehicle. Sun and Jing [17] constructed an n-layer scissor-like vibration isolator and analyzed its nonlinear characteristics for better performance in the horizontal and vertical directions. Han and Cao [18] combined a simple pendulum and a mass-spring oscillator to introduce a novel rotating pendulum for a better vibration attenuation behavior. Ji and Brown [19] explored the coexistence of bi-stable bifurcating solutions arisen in a time-delayed mechanical system after the occurrence of 2:1 resonant Hopf bifurcations. Kandil and El-Ganaini [20] reduced the rotating blade's vibrations via a PPF controller with time delay and showed the delay effects on the system behavior. Lavazec *et al.* [21] proved experimentally that the nonlinearity type in an absorber enhanced the vibration reduction behavior around the first resonance of the studied main system. Liu *et al.* [22] investigated the position and velocity feedback active controllers with time delay in a cantilever beam dynamical system with a carried mass. Wang *et al.* [23] dealt with ultra-sub-harmonics and sub-harmonics of a bio-inspired structure with an isolation system that could be applicable in several industrial applications. Awrejcewicz *et al.* [24] analyzed the probable internal resonance between a linear oscillator coupled to an absorber at primary resonance. Hamed *et al.* [25], [26] utilized the macro fiber composite in order to apply active control schemes for attenuating the rotating blade's unwanted vibrations. Liu *et al.* [27] investigated the chaos and resonance of MEMS and NEMS where the time delay effects were shown for achieving a safe operation. Salighe and Mohammadi [28] employed a virtual absorber at different spots of Timoshenko beams to guarantee the simultaneous suppression of the undesired oscillations. Kandil *et al.* [29], [30] have turned the quasi-periodic motion into a periodic one of a rotor active-magnetic-bearings model thanks to the presented tuned PPF and NSC controllers. Liu *et al.* [31] investigated different resonance cases along with time delay of controlling a clamped micro-beam coupled to an electrostatic micro-actuator. Mohanty and Dwivedy [32] carried out an active vibration absorption in order to suppress the vibrations of a single DOF spring-mass model which was exposed to both harmonic and parametric forces. Yan *et al.* [33] analyzed the multi-stability in a time-delayed cutting mechanical system including the statistical basins of attraction. Zhou *et al.* [34] focused on the dynamical performances of a two DOF magnetically coupled oscillators where the target component entered the saturated steady-state responses. Ma *et al.* [35], [36] presented a dual-predictive control algorithm depending on an adaptive error correction for the four-wire voltage source inverters where the error strategy was embedded into both the outer and inner prediction loop. They also introduced an event-triggered consensus control approach and built a nonlinear state-space function describing the AC micro-grid.

In this work, 2D and 3D plots are included to show the dynamical behavior of a mass-damper-spring model before and after control. This model is controlled with the help of linear variable differential transformer (LVDT) and servo-controlled linear actuator (SCLA). The control unit is provided with PPF control algorithm which gives acceptable minimum amplitudes for the car of mass m. The whole system dynamics and solutions are extracted via the well-known Krylov-Bogoliubov averaging perturbation method in order to define the amplitudes and phases of the car and PPF vibrations. The main contributions of this work are as follows: (1) the proposed controller suppresses the car's vibration amplitude to its lowest level, (2) the vibrations can be maintained at lowest levels regardless the change in the excitation frequency, (3) this can be done once the excitation frequency is measured and tuned with the controller's natural frequency, (4) the controller's damping can reduce any newly created vibration peak amplitudes in case of mistuning between the excitation and the controller frequencies, (5) 2D and 3D visualizations are included in order to picture a wide view of the whole system dynamics to the reader.

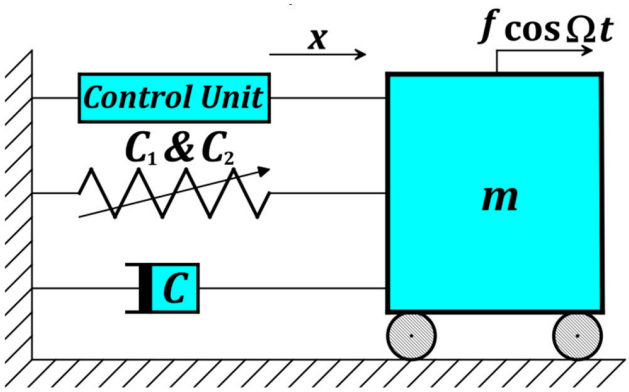

FIGURE 1. Mass-damper-spring model with a control unit.

II. MATHEMATICAL MODELING OF THE MASS-DAMPER-SPRING COMBINATION WITH A CONTROL UNIT

The studied mass-damper-spring model with a control unit is shown in Fig. 1. Here, the car of mass m is attached to a damper (dashpot) whose viscosity coefficient is C without mass and stiffness. The car is also attached to a spring having a linear and cubic-nonlinear stiffness C_1 and C_2, respectively, while its mass has been neglected. The car is subjected to a periodic excitation $f\cos(\Omega t)$. Newton's second law of motion leads us to get the model kinetics which can be represented by:

$$m\ddot{x}+C\dot{x}+C_1x+C_2x^3=f\cos(\Omega t)+U(t) \qquad (1)$$

where x is the car's displacement from an adequate equilibrium position and $U(t)$ is the control signal produced by the control unit. The studied model (Eq. (1)) is a lumped-parameter model which describes only the horizontal displacement ($x(t)$) of the car by a 2nd order ordinary differential equation. Hence, this model's dimension is finite and not high (specifically 1D). We did not resort to any dimensionality reduction method. Without generality loss, the control unit (shown in Fig. 2) comprises of a feedback module which is a linear variable differential transformer (LVDT) whose ferromagnetic-core is attached to the car so as to determine its position x efficiently. This transformer has three coils as shown where the primary coil is in the center and the other two secondary coils are at the terminals. The core (attached to the car) slides freely all over the LVDT axis. The primary coil is driven by an AC current in order to produce an induction voltage in each secondary coil which is proportional to the core length linking to that secondary coil. The connection of coils is designed to generate an output voltage V as a difference between the two secondary coils voltages. The output voltage V is proportional to the position of the car x so we need to make a signal conditioning in order to produce a suitable signal for the controller. The adopted PPF controller is a conventional robust vibration controller. We have chosen it according to the previously published Refs. [15], [20], [25], and [29] for its good results in reducing the vibrations efficiently. Herein, it is applied to minimize the car's unwanted oscillations. Its input is the feedback signal x while its output is the control signal y that is computed according to the following relation which is represented in Fig. 2:

$$\ddot{y}+\mu_c\dot{y}+\omega_c^2 y = k_c x \tag{2}$$

where μ_c is the PPF's damping coefficient, ω_c is its natural frequency and k_c is the feedback gain to be adjusted due to operation. We are coming to the final stage of actuation. The output signal y is amplified by a control gain k which can be also adjusted due to operation and the result is $U(t) = ky$. Then it is inserted into a power amplifier so as to generate the suitable current for the servo-controlled linear actuator (SCLA). This SCLA is some kind of a linear motor driven by the control signal $U(t)$ in order to make the push-pull motions required for controlling the car connected to it.

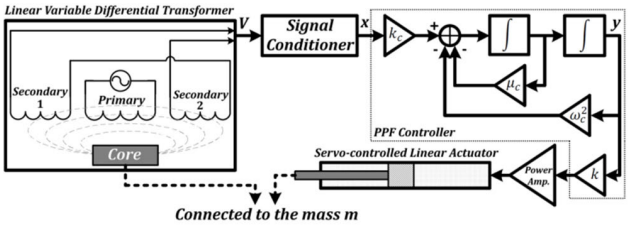

FIGURE 2. The control unit to be attached to the car of mass m.

In this work, we propose a theoretical approach of an adaptive feature for improving the traditional performance of this controller. This adaptation can be done by tuning the measured excitation frequency Ω to the controller's natural frequency ω_c in order to guarantee minimum vibratory amplitudes regardless of the excitation frequency. Simplifying Eq. (1) and writing it along with Eq. (2) yield

$$\ddot{x}+\mu\dot{x}+\omega^2 x+\alpha x^3 = f\cos(\Omega t)+ky \tag{3a}$$
$$\ddot{y}+\mu_c\dot{y}+\omega_c^2 y = k_c x \tag{3b}$$

where $\mu = C/m$, $\omega^2 = C_1/m$, $\alpha = C_2/m$, $f^* = f/m$, $k^* = k/m$. The asterisks have been omitted for brevity. To solve the system of nonlinear differential equations above, we can resort to the Krylov-Bogoliubov averaging perturbation method [37]. Before applying this method, let a small perturbation parameter ε be imposed on some parameters of Eqs. (3) such that $\mu = \varepsilon\hat{\mu}$, $\mu_c = \varepsilon\hat{\mu}_c$, $\alpha = \varepsilon\hat{\alpha}$, $f = \varepsilon\hat{f}$, $k = \varepsilon\hat{k}$, $k_c = \varepsilon\hat{k}_c$ in order to discriminate the free undamped linear problem from the one above as follows

$$\ddot{x}+\varepsilon\hat{\mu}\dot{x}+\omega^2 x+\varepsilon\hat{\alpha}x^3 = \varepsilon\hat{f}\cos(\Omega t)+\varepsilon\hat{k}y \tag{4a}$$
$$\ddot{y}+\varepsilon\hat{\mu}_c\dot{y}+\omega_c^2 y = \varepsilon\hat{k}_c x \tag{4b}$$

When $\varepsilon = 0$, the general solution of Eqs. (4) can be written as

$$x = a_1\cos(\omega t+\beta_1) \tag{5a}$$
$$y = a_2\cos(\omega_c t+\beta_2) \tag{5b}$$

where a_i and β_i are constants. Then,

$$\dot{x} = -\omega a_1\sin(\omega t+\beta_1) \tag{6a}$$
$$\dot{y} = -\omega_c a_2\sin(\omega_c t+\beta_2) \tag{6b}$$

When $\varepsilon \neq 0$, the solution in Eqs. (5) is expected to be the same but with a_i and β_i as time-varying. Taking the derivative of Eqs. (5) yields

$$\dot{x} = \dot{a}_1\cos(\omega t+\beta_1)-\omega a_1\sin(\omega t+\beta_1)-a_1\dot{\beta}_1\sin(\omega t+\beta_1) \tag{7a}$$
$$\dot{y} = \dot{a}_2\cos(\omega_c t+\beta_2)-\omega_c a_2\sin(\omega_c t+\beta_2)-a_2\dot{\beta}_2\sin(\omega_c t+\beta_2) \tag{7b}$$

Equalizing Eqs. (6) with (7) leads us to

$$\dot{a}_1\cos(\omega t+\beta_1)-a_1\dot{\beta}_1\sin(\omega t+\beta_1) = 0 \tag{8a}$$
$$\dot{a}_2\cos(\omega_c t+\beta_2)-a_2\dot{\beta}_2\sin(\omega_c t+\beta_2) = 0 \tag{8b}$$

Taking the derivative of Eqs. (6) yields

$$\ddot{x} = -\omega\dot{a}_1\sin(\omega t+\beta_1)-\omega^2 a_1\cos(\omega t+\beta_1) -\omega a_1\dot{\beta}_1\cos(\omega t+\beta_1) \tag{9a}$$
$$\ddot{y} = -\omega_c\dot{a}_2\sin(\omega_c t+\beta_2)-\omega_c^2 a_2\cos(\omega_c t+\beta_2) -\omega_c a_2\dot{\beta}_2\cos(\omega_c t+\beta_2) \tag{9b}$$

Substituting Eqs. (5), (6), and (9) into Eqs. (4) gives us

$$\dot{a}_1\sin(\omega t+\beta_1)+a_1\dot{\beta}_1\cos(\omega t+\beta_1) = -\varepsilon\hat{\mu}a_1\sin(\omega t+\beta_1)+\frac{\varepsilon\hat{\alpha}}{\omega}a_1^3\cos^3(\omega t+\beta_1) -\frac{\varepsilon\hat{f}}{\omega}\cos(\Omega t)-\frac{\varepsilon\hat{k}}{\omega}a_2\cos(\omega_c t+\beta_2) \tag{10a}$$

$$\dot{a}_2 \sin(\omega_c t+\beta_2)+a_2\dot{\beta}_2 \cos(\omega_c t+\beta_2) = -\varepsilon\hat{\mu}_c a_2 \sin(\omega_c t+\beta_2) - \frac{\varepsilon\hat{k}_c}{\omega_c} a_1 \cos(\omega t+\beta_1) \quad (10b)$$

Solving Eqs. (8) and (10) with using trigonometric identities and returning every scaled parameter to its original value lead to

$$\begin{aligned}\dot{a}_1 &= -\frac{\mu}{2}a_1+\frac{\mu}{2}a_1\cos(2\omega t+2\beta_1)+\frac{\alpha}{4\omega}a_1^3\sin(2\omega t+2\beta_1)\\ &+\frac{\alpha}{8\omega}a_1^3\sin(4\omega t+4\beta_1)-\frac{f}{2\omega}\sin((\omega-\Omega)t+\beta_1)\\ &-\frac{f}{2\omega}\sin((\omega+\Omega)t+\beta_1)-\frac{k}{2\omega}a_2\sin((\omega-\omega_c)t\\ &+\beta_1-\beta_2)-\frac{k}{2\omega}a_2\sin((\omega+\omega_c)t+\beta_1+\beta_2) \quad (11a)\\ a_1\dot{\beta}_1 &= -\frac{\mu}{2}a_1\sin(2\omega t+2\beta_1)+\frac{3\alpha}{8\omega}a_1^3+\frac{\alpha}{2\omega}a_1^3\cos(2\omega t+2\beta_1)\\ &+\frac{\alpha}{8\omega}a_1^3\cos(4\omega t+4\beta_1)-\frac{f}{2\omega}\cos((\omega-\Omega)t+\beta_1)\\ &-\frac{f}{2\omega}\cos((\omega+\Omega)t+\beta_1)-\frac{k}{2\omega}a_2\cos((\omega-\omega_c)t\\ &+\beta_1-\beta_2)-\frac{k}{2\omega}a_2\cos((\omega+\omega_c)t+\beta_1+\beta_2) \quad (11b)\\ \dot{a}_2 &= -\frac{\mu_c}{2}a_2+\frac{\mu_c}{2}a_2\cos(2\omega_c t+2\beta_2)-\frac{k_c}{2\omega_c}a_1\sin((\omega_c-\omega)t\\ &+\beta_2-\beta_1)-\frac{k_c}{2\omega_c}a_1\sin((\omega_c+\omega)t+\beta_2+\beta_1) \quad (11c)\\ a_2\dot{\beta}_2 &= -\frac{\mu_c a_2}{2}\sin(2\omega_c t+2\beta_2)-\frac{k_c}{2\omega_c}a_1\cos((\omega-\omega_c)t\\ &+\beta_1-\beta_2)-\frac{k_c}{2\omega_c}a_1\cos((\omega+\omega_c)t+\beta_1+\beta_2) \quad (11d)\end{aligned}$$

For seeking the first approximation solution, we keep only the slowly-varying terms on the right-hand sides of Eqs. (11) where they can be considered constant in the interval $[0, \pi]$. For a simultaneous resonance case ($\Omega \approx \omega$, $\omega_c \approx \omega$), Eqs. (11) will be

$$\begin{aligned}\dot{a}_1 &= -\frac{\mu}{2}a_1-\frac{f}{2\omega}\sin((\omega-\Omega)t+\beta_1)\\ &-\frac{k}{2\omega}a_2\sin((\omega-\omega_c)t+\beta_1-\beta_2) \quad (12a)\\ a_1\dot{\beta}_1 &= \frac{3\alpha}{8\omega}a_1^3-\frac{f}{2\omega}\cos((\omega-\Omega)t+\beta_1)\\ &-\frac{k}{2\omega}a_2\cos((\omega-\omega_c)t+\beta_1-\beta_2) \quad (12b)\\ \dot{a}_2 &= -\frac{\mu_c}{2}a_2-\frac{k_c}{2\omega_c}a_1\sin((\omega_c-\omega)t+\beta_2-\beta_1) \quad (12c)\\ a_2\dot{\beta}_2 &= -\frac{k_c}{2\omega_c}a_1\cos((\omega-\omega_c)t+\beta_1-\beta_2) \quad (12d)\end{aligned}$$

Expressing the closeness of frequencies in the studied resonance case by the detuning parameters σ and σ_c as follows

$$\sigma = \Omega-\omega \quad (13a)$$
$$\sigma_c = \omega_c-\omega \quad (13b)$$

Substituting Eqs. (13) into (12) yields the following autonomous system of DEs:

$$\begin{aligned}\dot{a}_1 &= -\frac{\mu}{2}a_1+\frac{f}{2\omega}\sin\phi_1+\frac{k}{2\omega}a_2\sin(\phi_1-\phi_2) \quad (14a)\\ a_1\dot{\phi}_1 &= \sigma a_1-\frac{3\alpha}{8\omega}a_1^3+\frac{f}{2\omega}\cos\phi_1+\frac{k}{2\omega}a_2\cos(\phi_1-\phi_2) \quad (14b)\\ \dot{a}_2 &= -\frac{\mu_c}{2}a_2-\frac{k_c}{2\omega_c}a_1\sin(\phi_1-\phi_2) \quad (14c)\\ a_2\dot{\phi}_2 &= (\sigma-\sigma_c)a_2+\frac{k_c}{2\omega_c}a_1\cos(\phi_1-\phi_2) \quad (14d)\end{aligned}$$

where $\phi_1 = \sigma t-\beta_1$ and $\phi_2 = (\sigma-\sigma_c)t-\beta_2$. We need to study the steady-state behavior of the system, or in other words, we need to get the fixed points of Eqs. (14). It can be done by supposing that the fluctuations in both a_i and ϕ_i are zero, i.e. $\dot{a}_i = \dot{\phi}_i = 0$. This leads to

$$\begin{aligned}\mu a_{1s} &= \frac{f}{\omega}\sin\phi_{1s}+\frac{k}{\omega}a_{2s}\sin(\phi_{1s}-\phi_{2s}) \quad (15a)\\ -2\sigma a_{1s}+\frac{3\alpha}{4\omega}a_{1s}^3 &= \frac{f}{\omega}\cos\phi_{1s}+\frac{k}{\omega}a_{2s}\cos(\phi_{1s}-\phi_{2s}) \quad (15b)\\ \mu_c a_{2s} &= -\frac{k_c}{\omega_c}a_{1s}\sin(\phi_{1s}-\phi_{2s}) \quad (15c)\\ -2(\sigma-\sigma_c)a_{2s} &= \frac{k_c}{\omega_c}a_{1s}\cos(\phi_{1s}-\phi_{2s}) \quad (15d)\end{aligned}$$

where a_{is} and ϕ_{is} are the steady values of a_i and ϕ_i, respectively. Solving Eqs. (15c) and (15d) gives us

$$a_{1s} = \frac{\omega_c}{k_c}\sqrt{\mu_c^2+4(\sigma-\sigma_c)^2}a_{2s} = \gamma a_{2s} \quad (16)$$

Solving Eqs. (15c) with (15a), and (15d) with (15b) leads to

$$\begin{aligned}\mu\omega a_{1s}^2+\frac{k\mu_c\omega_c}{k_c}a_{2s}^2 &= f a_{1s}\sin\phi_{1s} \quad (17a)\\ -2\sigma\omega a_{1s}^2+\frac{3\alpha}{4}a_{1s}^4+\frac{2(\sigma-\sigma_c)k\omega_c}{k_c}a_{2s}^2 &= f a_{1s}\cos\phi_{1s} \quad (17b)\end{aligned}$$

Solving Eqs. (17) to Eliminate ϕ_{1s} with using (16) gives the sextic equation in a_{1s} and a_{2s} as follows:

$$\begin{aligned}\gamma_1 a_{1s}^6+\gamma_2 a_{1s}^4+\gamma_3 a_{1s}^2+\gamma_4 &= 0 \quad (18a)\\ \gamma_1\gamma^6 a_{2s}^6+\gamma_2\gamma^4 a_{2s}^4+\gamma_3\gamma^2 a_{2s}^2+\gamma_4 &= 0 \quad (18b)\end{aligned}$$

where

$$\begin{aligned}\gamma_1 &= \frac{9\alpha^2}{16}\\ \gamma_2 &= \frac{3\alpha}{2}\left[\frac{2(\sigma-\sigma_c)k\omega_c}{k_c\gamma^2}-2\sigma\omega\right]\\ \gamma_3 &= \left[\mu\omega+\frac{k\mu_c\omega_c}{k_c\gamma^2}\right]^2+\left[\frac{2(\sigma-\sigma_c)k\omega_c}{k_c\gamma^2}-2\sigma\omega\right]^2\\ \gamma_4 &= -f^2\end{aligned}$$

The solutions of Eqs. (18) along with (16) obtain the steady-state amplitudes a_{is}. On the other hand of this analysis, the steady-state amplitudes a_{is} and phases ϕ_{is} should be tested for stability so as to check whether they are

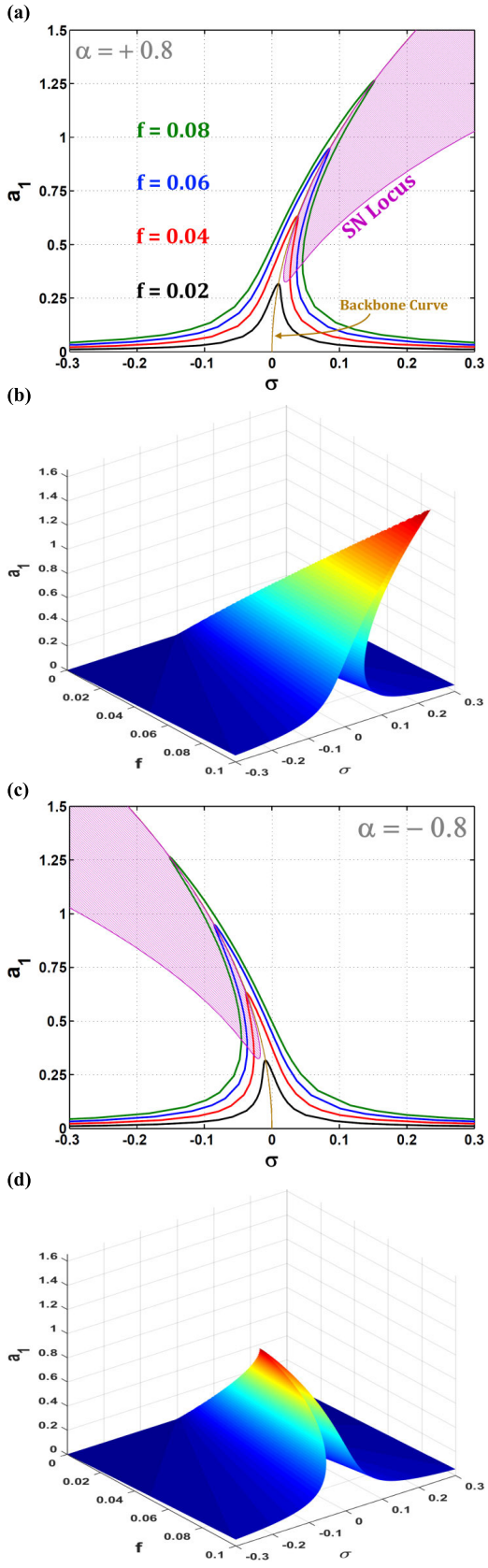

FIGURE 3. Response curves of the mass m to the excitation frequency detuning σ at variant excitation force f before control (k = 0 and $\alpha = \{+0.8, -0.8\}$): (a, c) 2D plot, (b, d) 3D plot.

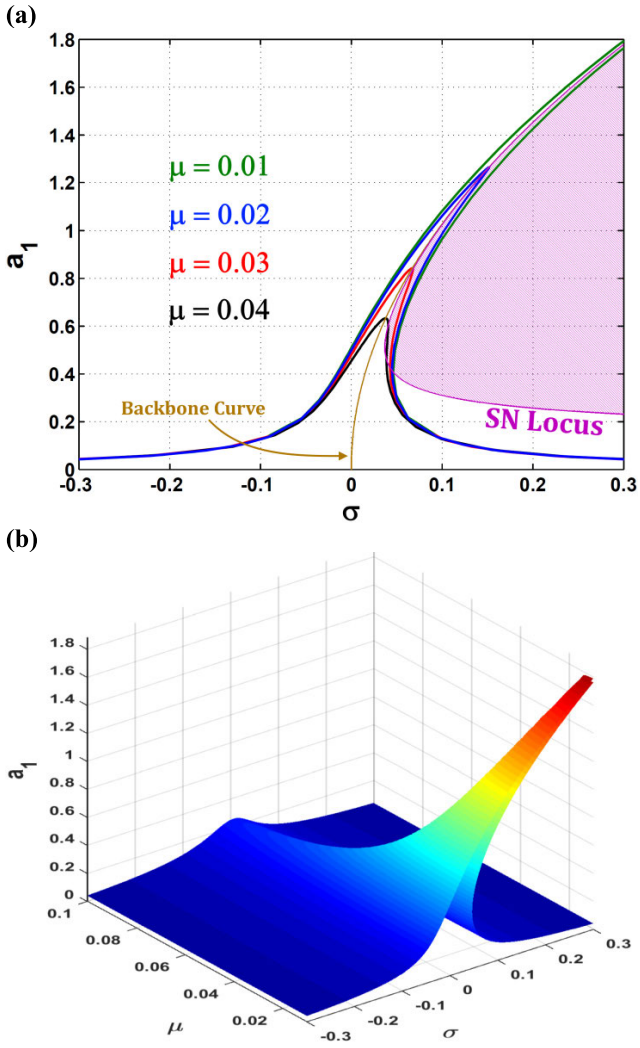

FIGURE 4. Response curves of the mass m to the excitation frequency detuning σ at variant damping μ before control (k = 0): (a) 2D plot, (b) 3D plot.

stable or not. It can be easily known via the characteristic equation's eigenvalues of Eqs. (14) in terms of small disturbances around the fixed points [38]. If all of the real parts of the computed eigenvalues are negative, the steady-state solution is asymptotically stable, otherwise it is unstable. Moreover, the bifurcation will happen if an eigenvalue traverses the imaginary axis of the complex plane.

III. RESULTS AND DISCUSSION

Herein, the mass-damper-spring dynamics can be discussed via several plots before and after activating the control unit. The plots clarify the influences of different parameters on the model's frequency- and force-response-curves. Furthermore, 3D plots are included to give a wider view of the model's behavior before and after control. The adopted dimensionless parameters in the model's operation are chosen as: $\mu = 0.02$,

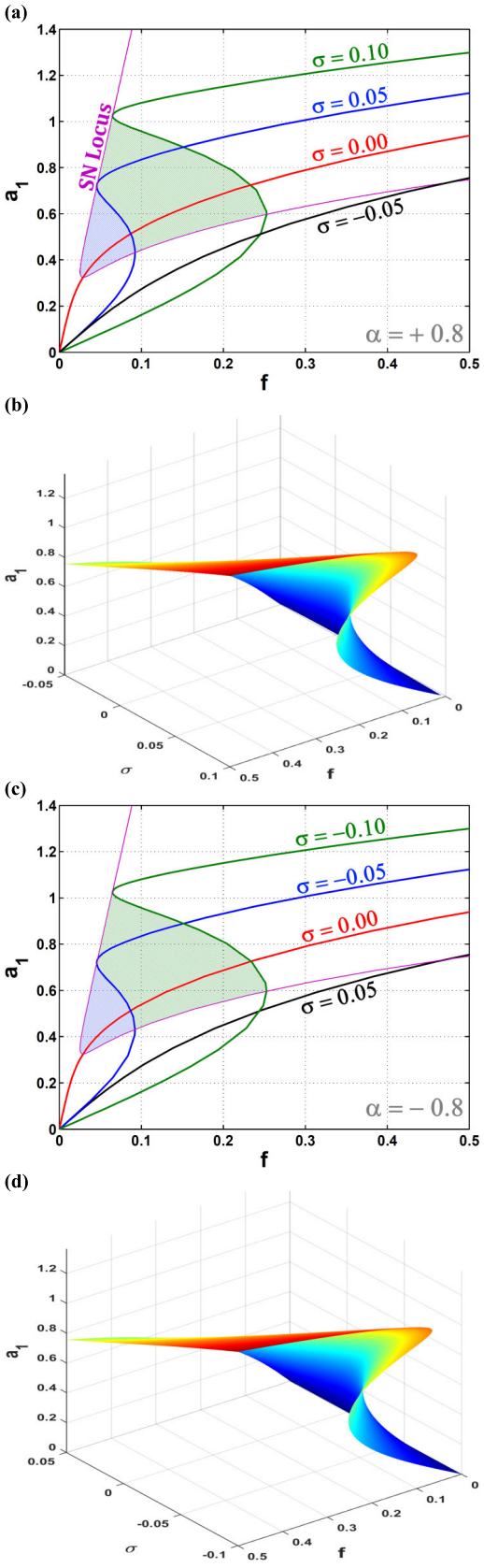

FIGURE 5. Response curves of the mass m to the excitation force f at variant frequency detuning σ before control (k = 0 and $\alpha = \{+0.8, -0.8\}$): (a, c) 2D plot, (b, d) 3D plot.

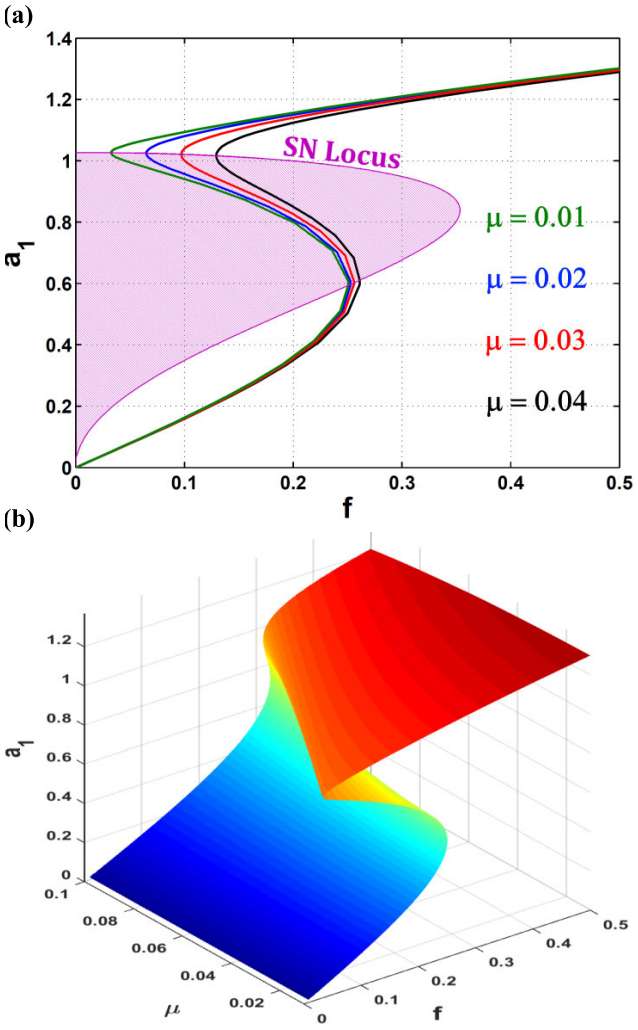

FIGURE 6. Response curves of the mass m to the excitation force f at variant damping μ before control (k = 0): (a) 2D plot, (b) 3D plot.

$\omega = \sqrt{10} \cong 3.1623$, $\sigma \in [-0.3, 0.3]$, $\Omega = \omega + \sigma$, $\alpha = 0.8$, $f = 0.06$, $k = k_c = 1.5$, $\mu_c = 0.001$, $\sigma_c \in [-0.3, 0.3]$, $\omega_c = \omega + \sigma_c$, unless otherwise changed. In Fig. 3, the response curves of the mass m's vibrational amplitude a_1 to the excitation frequency detuning σ are shown before applying the control unit ($k = 0$) at different values of the excitation force f. It is clear that the mass m's amplitude responds linearly for small values of f in Fig. 3a. As long as the force f increases, the curve leans to the right denoting a nonlinear hardening phenomenon. In this case, the mass m may follow one of the multiple solutions until it jumps off from it to another one when the curve's tangent becomes vertical. This is where the Saddle-Node (SN) bifurcation point exists. For generality, the locus of all possible SN points is plotted at variant f to contain the unstable branches where the mass m cannot approach. Also, we have indicated the backbone curve in order to view the locus of maxima of the shown curves. On the other hand in Fig. 3b, the 3D surface

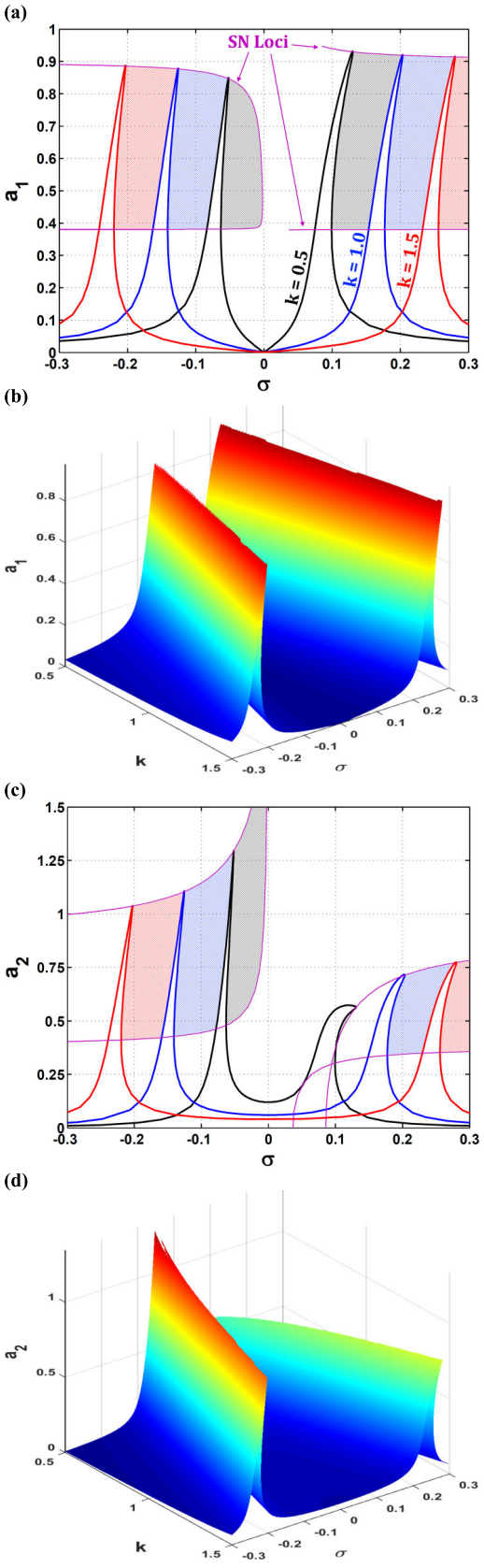

FIGURE 7. Response curves of the mass m (a, b) and the PPF controller (c, d) to σ at variant k with f = 0.06.

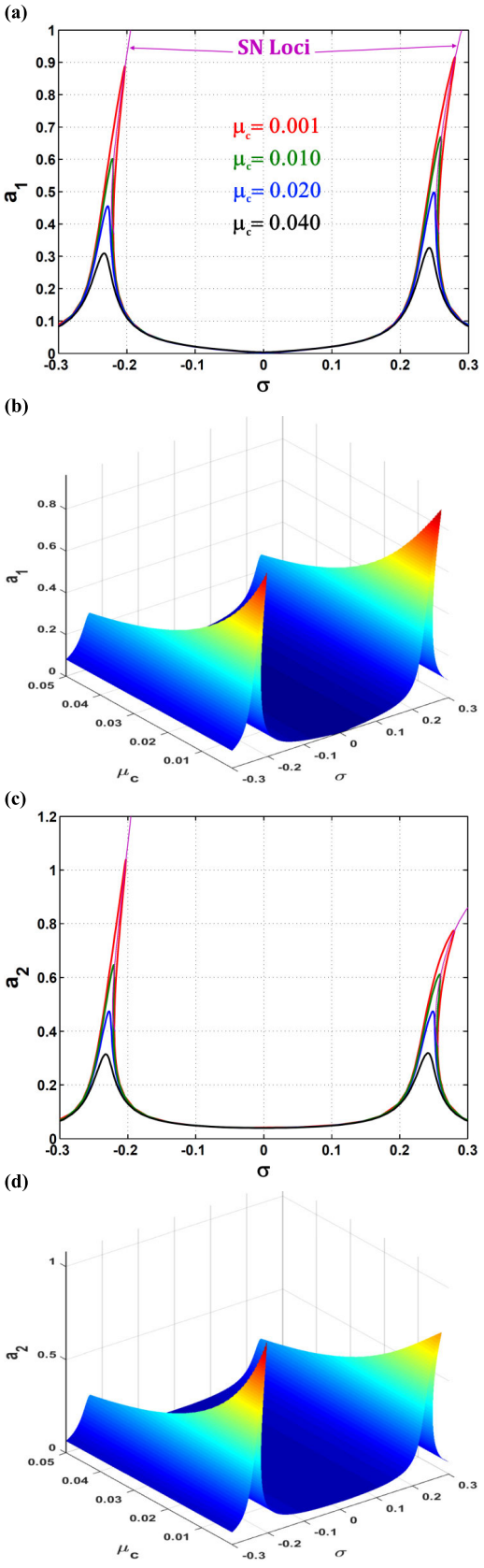

FIGURE 8. Response curves of the mass m (a, b) and the PPF controller (c, d) to σ at variant controller damping μ_c with f = 0.06 and k = 1.5.

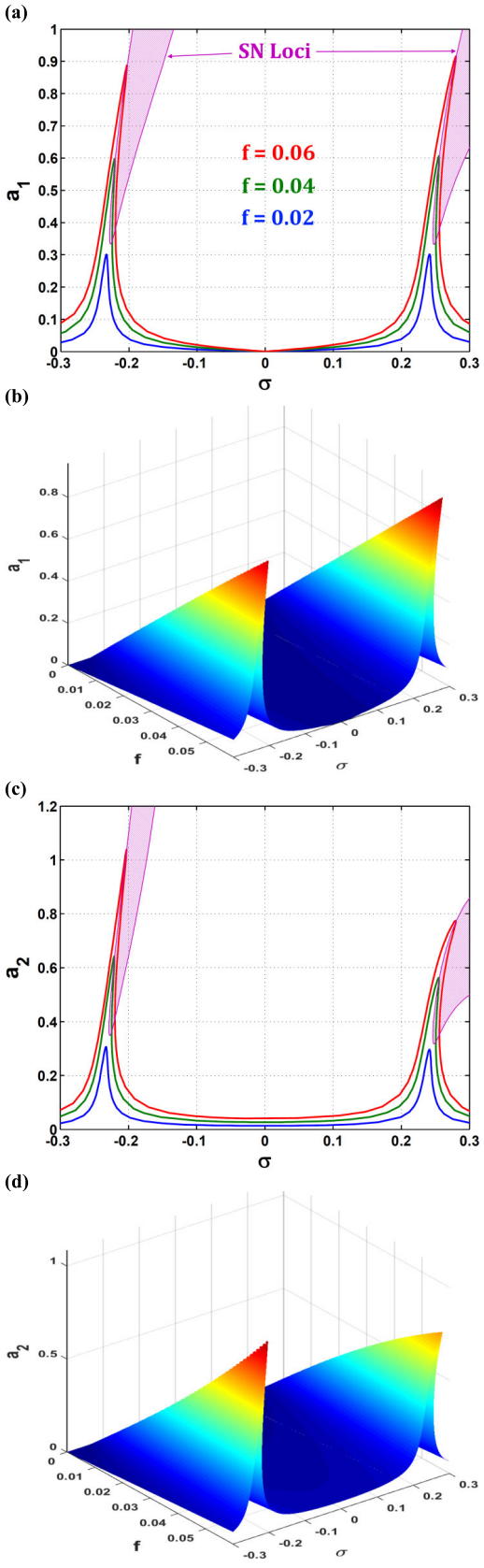

FIGURE 9. Response curves of the mass m (a, b) and the PPF controller (c, d) to σ at variant f with k = 1.5.

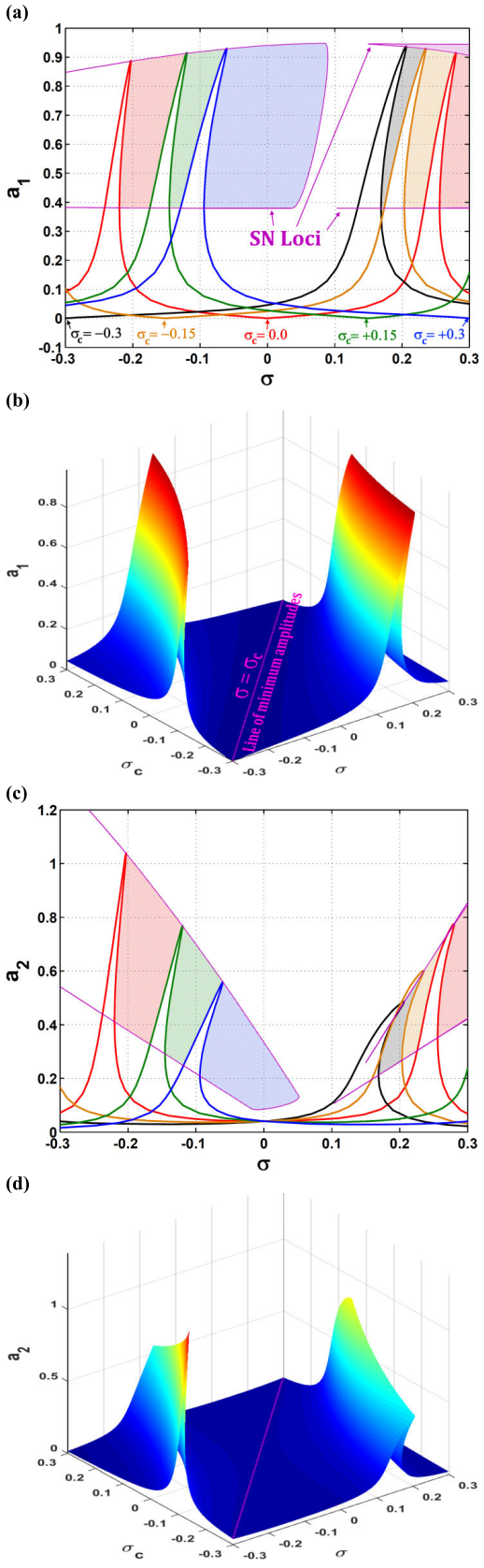

FIGURE 10. Response curves of the mass m (a, b) and the PPF controller (c, d) to σ at variant controller frequency detuning σ_c with f = 0.06 and k = 1.5.

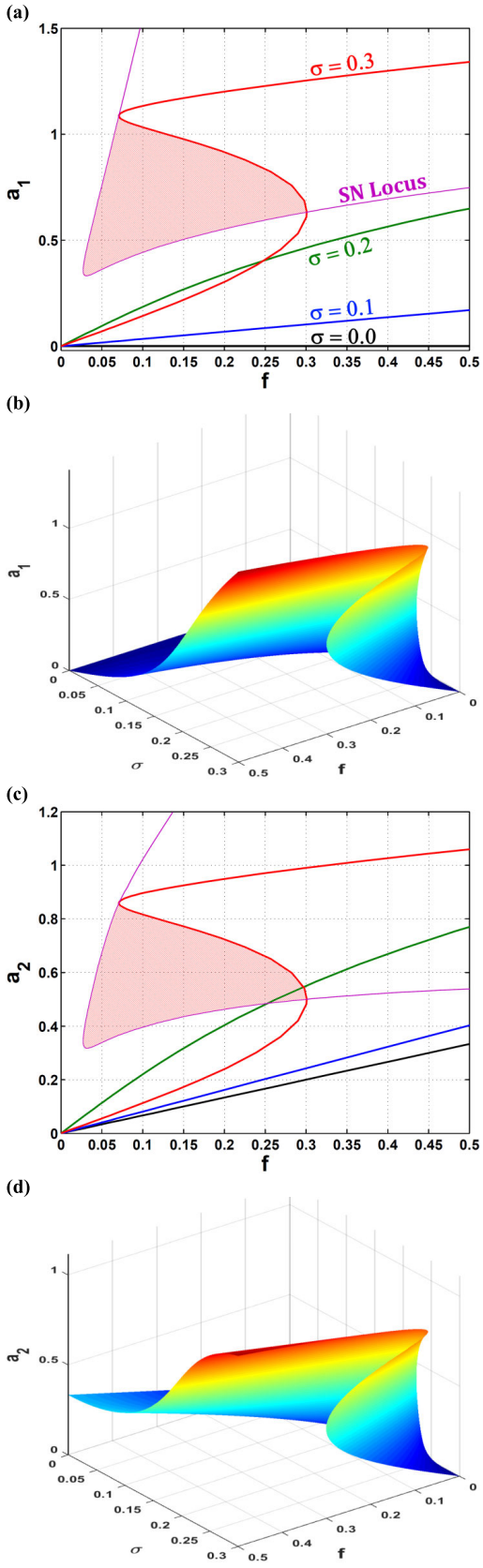

FIGURE 11. Response curves of the mass m (a, b) and the PPF controller (c, d) to f at variant σ with k = 1.5 and $\sigma_c = 0.0$.

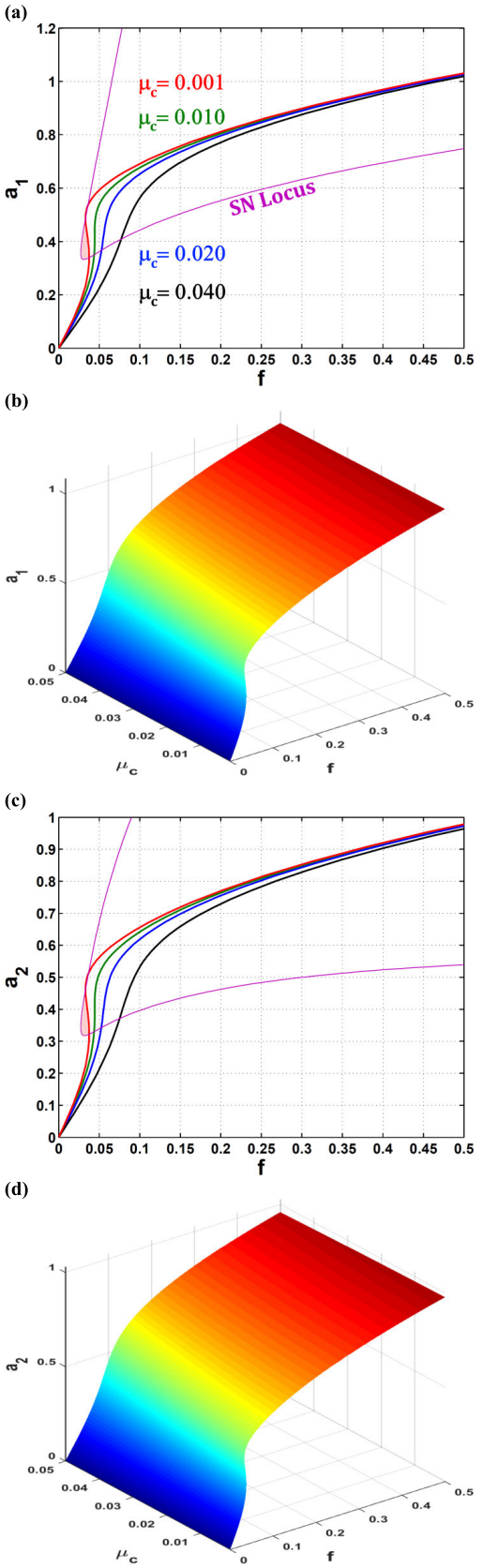

FIGURE 12. Response curves of the mass m (a, b) and the PPF controller (c, d) to f at variant μ_c with k = 1.5, $\sigma = 0.25$, and $\sigma_c = 0.0$.

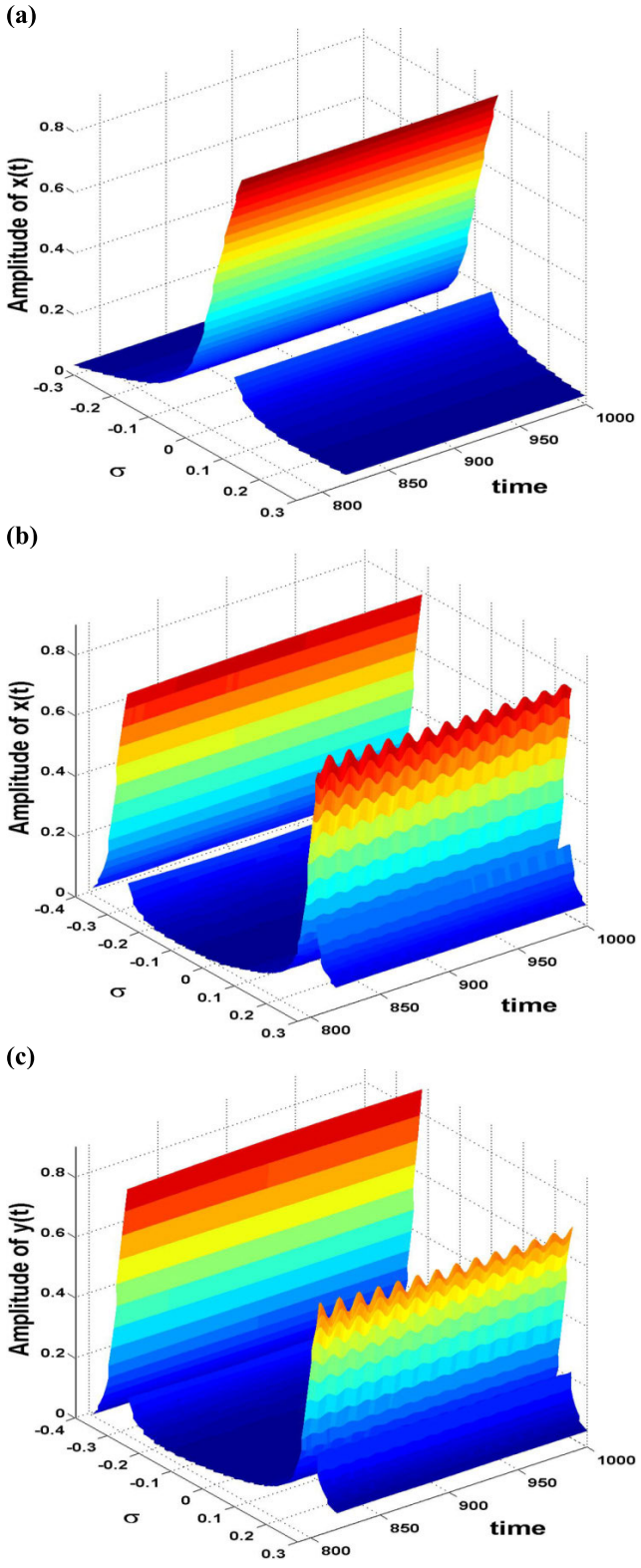

FIGURE 13. 3D visualization of the time-frequency simulation of: (a, b) the mass m's amplitude, and (c) the PPF controller's amplitude at f = 0.06, k=1.5, and $\sigma_c = 0.0$ before and after control.

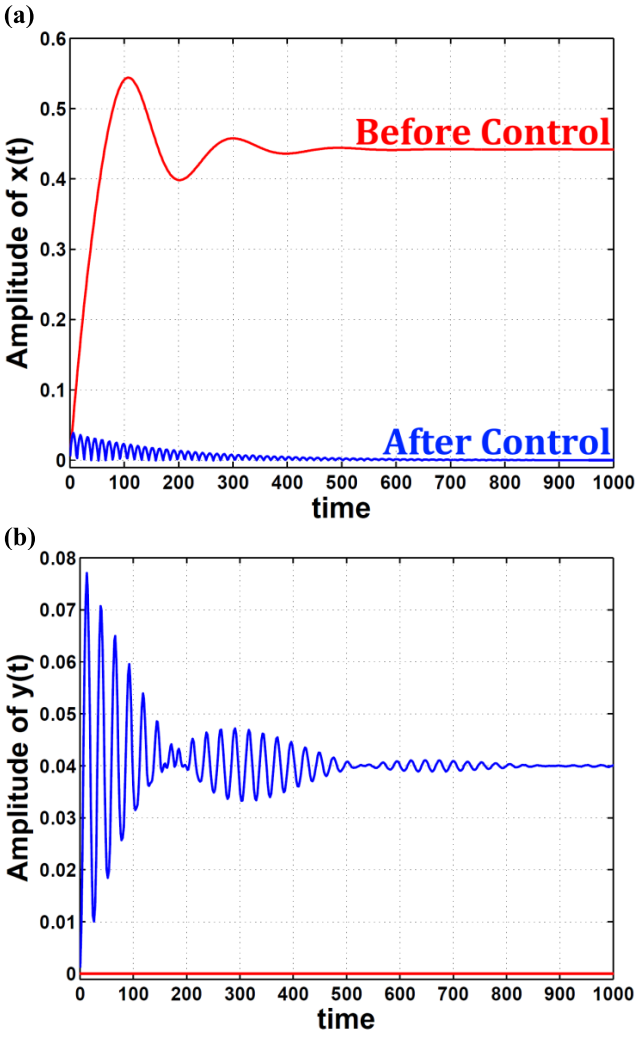

FIGURE 14. Comparison between the time responses of (a) the mass m's amplitude, and (b) the controller's amplitude at f = 0.06 and $\sigma \mathcal{D} 0$ before and after control.

defines the dependence of a_1 on both σ and f. This is a comprehensive view of Fig. 3a to show the direct influence of σ and f on the amplitude value and jump phenomena. Also, Figs. 3c and 3d clarify how the negativity of the nonlinearity parameter α converts the hardening effect to softening effect where the right-bending is now left-bending with the same force variability of Fig. 3a as shown. For clarity, the top of the surface is indicated by dark red color while the bottom is indicated by dark blue color as shown.

Figure 4 presents the response curves of the mass m's vibrational amplitude a_1 to the excitation frequency detuning σ before applying the control unit ($k = 0$) at different values of the damping μ. It is well-known from the modern control theory that the damping coefficient can attenuate (or damps) the output signal. This is clear in the figure where increasing the damping μ has reduced the maxima of the curves and also the intersection with the SN locus.

In Fig. 5, the effect of varying σ appears on the response curves of the mass m vibration amplitude a_1 to the force f before control. We can notice that the variability of σ from -0.05 to 0.10 can exhibit the appearance of SN points and also jump phenomena just as described in Fig. 3a.

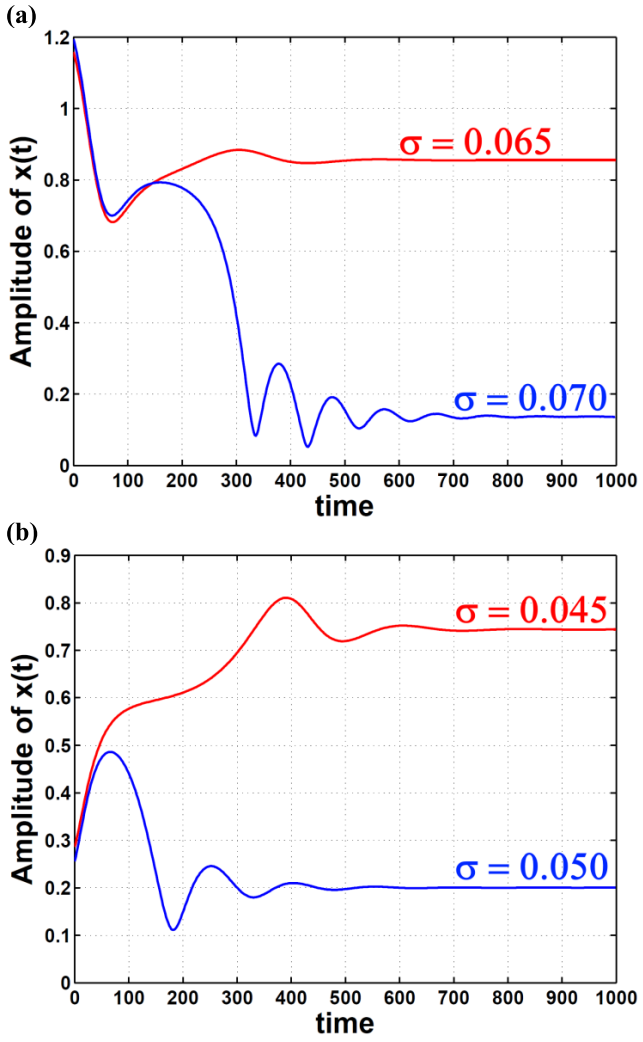

FIGURE 15. Time response simulation of the mass m's amplitude subjected to jump phenomena before control during: (a) sweeping σ up, (b) sweeping σ down.

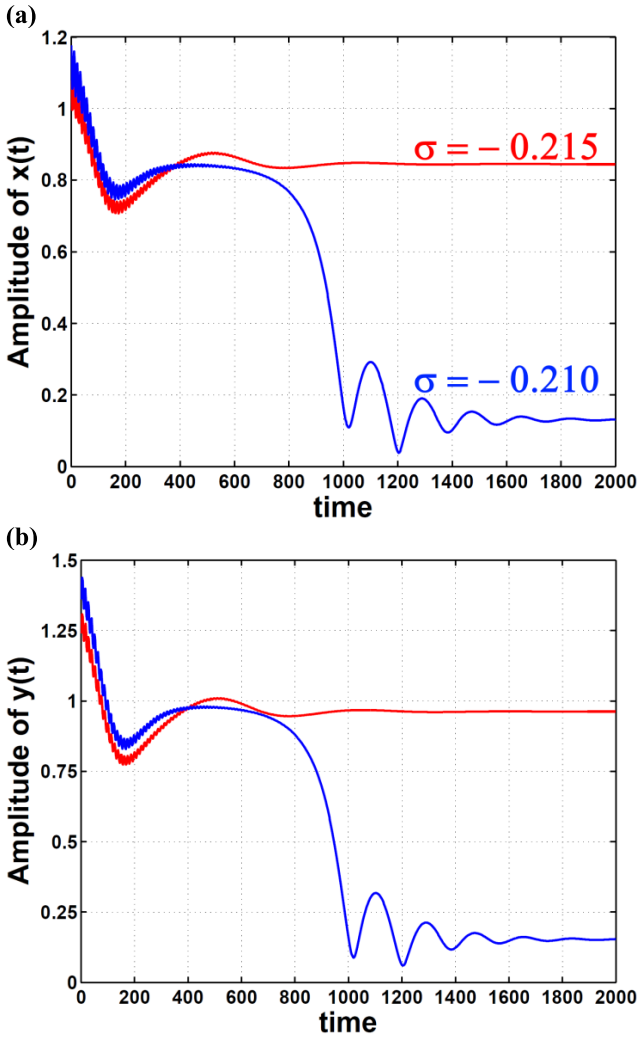

FIGURE 16. Time response simulation of: (a) the mass, and (b) the controller amplitudes subjected to jump phenomenon at the left peak during sweeping σ up.

This variability modifies also the curve shape from linear case to nonlinear case of the amplitude values doubled. The SN locus is plotted to show the path of vertical tangents. Figure 5b shows the 3D surface of such relation in Fig. 5a. Also, Figs. 5c and 5d show the softening effect at $\alpha = -0.8$ where the reverse variability of σ from 0.05 to -0.10 can generate SN points and jump phenomena just as described in Fig. 3c. Furthermore, Fig. 6 clarifies what has been discussed in Fig. 4 about the damping effect of μ but here is on the response curves to the force f. The damping effect is explicit in lowering the gap between the vertical tangents' points (SN points) which is a utility in quite avoiding the jump phenomena.

From now on, we are going to discuss the effect of control unit on the vibrational amplitudes of mass m when $k \neq 0$. Figure 7 portrays the response curves of both the mass m and the PPF controller to the frequency detuning σ at different values of the control gain k. We are keeping the equality that $k = k_c$ in all of the following figures. As can be seen in Figs. 7a and b, the single peak (which was before control) has been split into double peaks separated by something like a canyon. This canyon's width can be controlled by the value of the control gain k as shown. The larger the gain k is, the wider the canyon is. There is a utility which is the middle point in this canyon is the minimum amplitude point that we wish to force the mass m to stay at. You should not forget that the loci of the vertical tangents have been included there for indicating the SN points locations. Figures 7c and d show also the PPF controller amplitudes behavior with σ and k where the canyon appears also and is controlled by adjusting k.

Figure 8 demonstrates how the controller damping μ_c can affect the generated peaks amplitudes for both the mass m and the PPF vibrational amplitudes. This can be considered an advantage for suppressing the dual peaks amplitudes in case that σ has deviated to any one of the peaks. It is also evident in the 3D plots that increasing μ_c suppresses the peaks to acceptable levels.

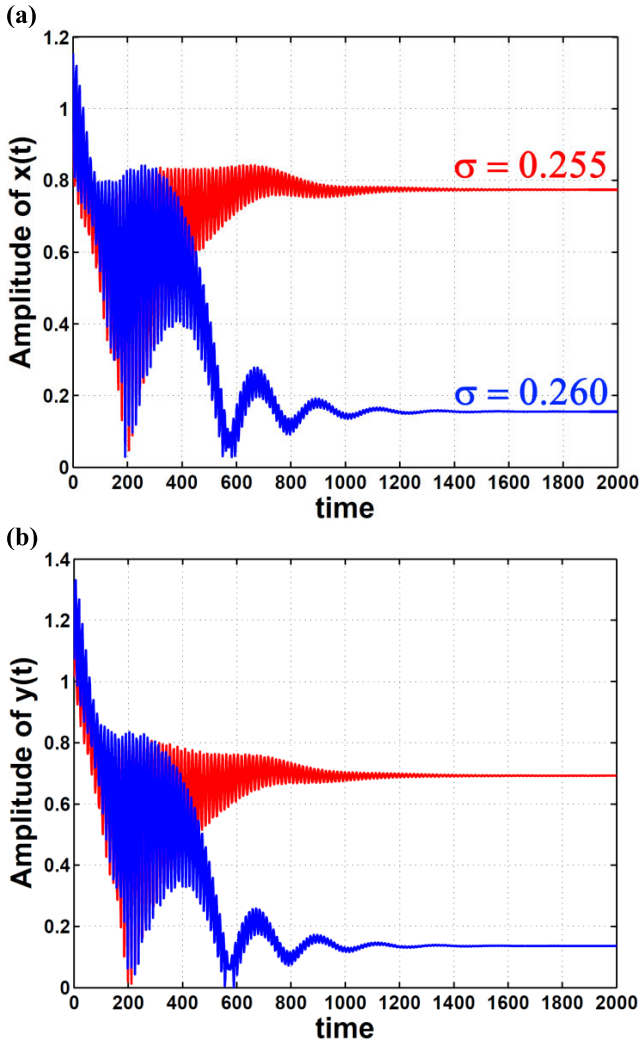

FIGURE 17. Time response simulation of: (a) the mass, and (b) the controller amplitudes subjected to jump phenomenon at the right peak during sweeping σ up.

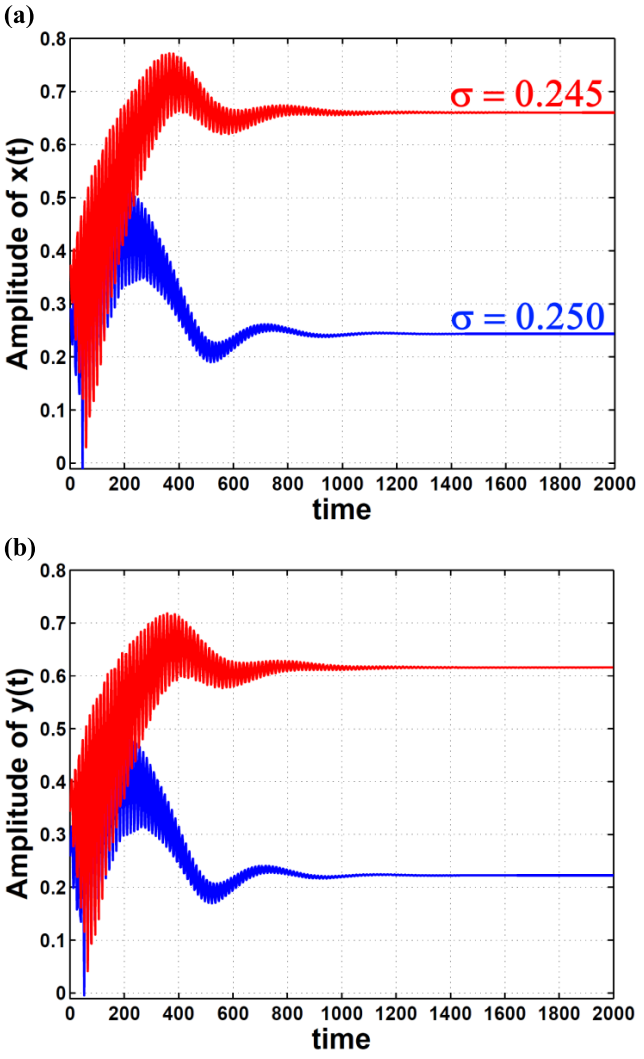

FIGURE 18. Time response simulation of: (a) the mass, and (b) the controller amplitudes subjected to jump phenomenon at the right peak during sweeping σ down.

Again, the effect of the force f on the response curves of the mass and the controller is shown in Fig. 9 at $k = 1.5$. It is clear that the peaks amplitudes are monotonically increasing in the excitation force f. This is very harmful at the peaks even after control. The good thing is that the middle point of the canyon (minimum amplitude point) has not been affected by the variant excitation force.

In the previous discussion, we were talking about the possibility of forcing the mass m to stay at the minimum amplitude point in order to avoid the high peaks in case of σ deviation away from zero. The following figure is the clue. Figure 10 presents the response curves of the mass and the controller to σ at different values of σ_c. It can be seen from Figs. 10a and c that the mass m and the controller can exhibit minimum amplitudes not only at $\sigma = 0$ but at different values of σ on one condition which is $\sigma = \sigma_c$. The chosen values of σ_c in the figure are $\sigma_c = -0.30, -0.15, 0.0, +0.15$, and $+0.30$ in order to show the reader different cases where the minimum amplitudes are at $\sigma = -0.30, -0.15, 0.0, +0.15$, and $+0.30$, respectively. This is so obvious in Figs. 10b and d where the minimum amplitudes of the mass and the controller can be reached on the line of $\sigma = \sigma_c$ as shown. The idea in guaranteeing the condition $\sigma = \sigma_c$ is evident in Eq. (13) where it can be achieved only if $\Omega = \omega_c$. This can be practically fulfilled if we can measure the excitation frequency Ω and provide this value to the PPF controller (Fig. 2) instead of ω_c. At this moment, the relation $\sigma = \sigma_c$ can be guaranteed in order to have minimum vibrational amplitudes for the mass m.

Figure 11 shows the relation between the excitation force and the output amplitudes of the mass and the controller at different values of excitation frequency detuning σ where the controller detuning $\sigma_c = 0$. We can notice that the mass barely vibrates at $\sigma = 0$ while the whole vibrations have been transferred to the PPF controller. However, the mass's vibrations increase as σ deviates from zero as shown and the

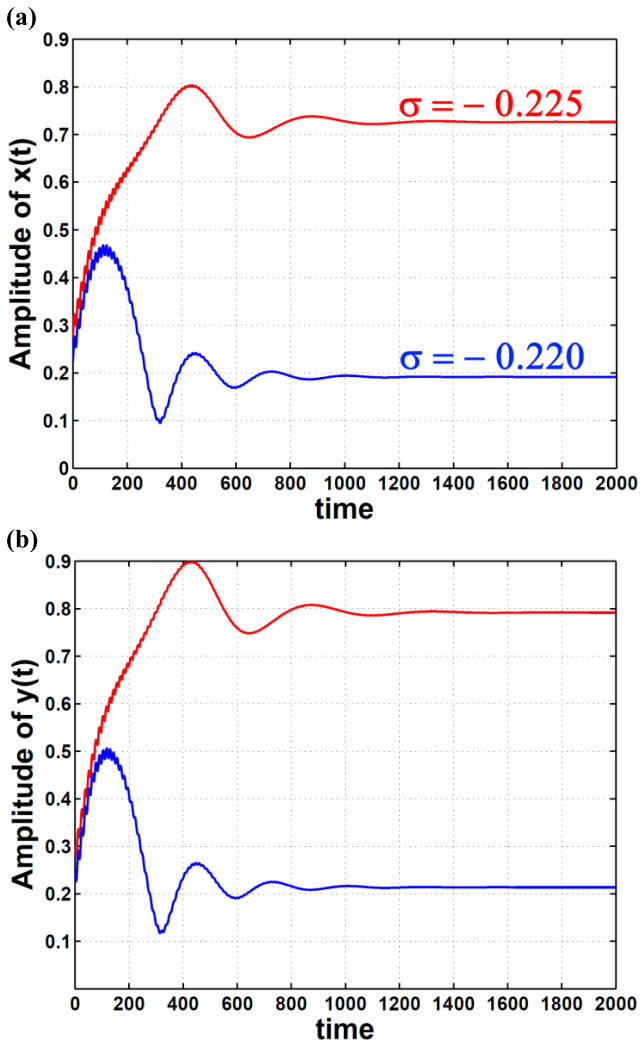

FIGURE 19. Time response simulation of: (a) the mass, and (b) the controller amplitudes subjected to jump phenomenon at the left peak during sweeping σ down.

jump phenomena are produced once again. In case you have noticed, the minimum vibratory level can be reached only if $\sigma = \sigma_c$ as we stated before regardless the value of f. The corresponding 3D plots confirm such behaviors. On the other hand in Fig. 12, the controller damping μ_c can slightly damp the f-response curves in order to avoid a vertical tangents region at one of the produced peaks (at $\sigma = 0.25$ and $\sigma_c = 0$) as shown.

Figures 13 to 19 portray a confirmation of the previously plotted figures using the 4th order Runge-Kutta numerical technique. Figure 13 show a 3D visualization of a time-frequency response of the actual peak amplitudes of the mass m and the controller for the last 100 peaks of 1000-seconds time signals. Before control in Fig. 13a, we can see the actual jump phenomena in the range $\sigma \in [0.05, 0.065]$ where we have discussed in Figs. 3 and 4. After control in Figs. 13b and c, the minimum amplitudes can be reached at $\sigma = 0$ while there are dual peaks with new jump phenomena in the range $\sigma \in \{[-0.225, -0.210] \cup [0.245, 0.260]\}$. Figures 14 to 19 show the 2D time history sections of Fig. 13 to clarify the system states before and after control and to depict all of the jump phenomena shown in Fig. 13.

IV. CONCLUSION

In this paper, 2D and 3D plots were included to show the dynamical behavior of a mass-damper-spring model before and after control. This model was controlled with the help of LVDT and SCLA. The control unit was provided with PPF control algorithm which gave acceptable minimum amplitudes for the car of mass m. The whole system dynamics and solutions were extracted via the well-known Krylov-Bogoliubov averaging perturbation method in order to define the amplitudes and phases of the car and PPF vibrations. Some concluded points could be summarized as follows:

A. THE CASE BEFORE ACTIVATING THE CONTROL UNIT

1) The mass m's amplitude responded linearly to small values of the excitation force f.
2) As long as f increased, the frequency-response curve leant to the right denoting a nonlinear hardening phenomenon.
3) Hence, the mass m might follow one of the multiple solutions until it had jumped off from it to another one when the curve's tangent became vertical (where the SN bifurcation point existed).
4) The damping coefficient μ could attenuate the curves maxima and also the intersection with the SN locus.
5) The variability of frequency detuning σ from -0.05 to 0.10 could exhibit the SN points and also jump phenomena in the force-response curve.
6) On the force-response curve, the parameter μ has lowered the gap between the SN points which was a utility in avoiding the jump phenomena.

B. THE CASE AFTER ACTIVATING THE CONTROL UNIT

1) On the force-response curve, the single peak of the pre-control case was split into dual peaks separated by a canyon whose width could be controlled by the control gain k.
2) That canyon's middle point has been the minimum amplitude point that we wished the mass m to stay at.
3) The controller damping μ_c could suppress the generated dual peaks amplitudes.
4) The mass m and the controller could exhibit minimum amplitudes not only at $\sigma = 0$ but also at different values of σ on one condition that $\sigma = \sigma_c$.
5) That could be practically fulfilled if Ω was measured and provided to the control unit instead of ω_c.
6) The mass m barely vibrated at $\sigma = 0$ while the whole vibrations have been transferred to the controller.
7) In case of mistuning ($\sigma \neq \sigma_c$), the mass vibrations increased as σ deviated from zero and the jump phenomena were produced once again.

8) The parameter μ_c could slightly damp the f-response curves in order to avoid a vertical tangents region at one of the produced dual peaks.

1) OUR FUTURE WORK INCLUDES

1) A study on the distributed-parameter system of an infinite-dimension to be reduced to a finite-dimension model.
2) Delay times to be involved in both feedback and control signals.
3) Implementation of an adaptive controller in order to confront more disturbances of different types.

CONFLICTS OF INTEREST

The authors declared no potential conflicts of interest with respect to the research, authorships, and/or publication of this article.

ACKNOWLEDGMENT

This research was supported by Taif University Researchers Supporting Project Number (TURSP-2020/96), Taif University, Taif, Saudi Arabia. This research was also supported by the National Science Centre, Poland, under the Grant OPUS 14 No. 2017/27/B/ST8/01330.

REFERENCES

[1] J. C. Ji and N. Zhang, "Suppression of the primary resonance vibrations of a forced nonlinear system using a dynamic vibration absorber," *J. Sound Vibrat.*, vol. 329, no. 11, pp. 2044–2056, May 2010, doi: 10.1016/j.jsv.2009.12.020.

[2] J. C. Ji and N. Zhang, "Suppression of super-harmonic resonance response using a linear vibration absorber," *Mech. Res. Commun.*, vol. 38, no. 6, pp. 411–416, Sep. 2011, doi: 10.1016/j.mechrescom.2011.05.014.

[3] F. M. Alsaleem and M. I. Younis, "Stabilization of electrostatic MEMS resonators using a delayed feedback controller," *Smart Mater. Struct.*, vol. 19, no. 3, Mar. 2010, Art. no. 035016, doi: 10.1088/0964-1726/19/3/035016.

[4] M. Febbo, "Harmonic response of a class of finite extensibility nonlinear oscillators," *Phys. Scripta*, vol. 83, no. 6, Jun. 2011, Art. no. 065009, doi: 10.1088/0031-8949/83/06/065009.

[5] J. C. Ji, X. Y. Li, Z. Luo, and N. Zhang, "Two-to-one resonant Hopf bifurcations in a quadratically nonlinear oscillator involving time delay," *Int. J. Bifurcation Chaos*, vol. 22, no. 3, Mar. 2012, Art. no. 1250060, doi: 10.1142/S0218127412500605.

[6] C. Liu, J. Qiu, H. Sun, Z. Wang, and H. Ji, "Nonlinear vibrations of beams with spring and damping delayed feedback control," *J. Vibroeng.*, vol. 15, pp. 340–354, Mar. 2013.

[7] C. Bavastri, M. Febbo, V. Gonçalves, and E. Lopes, "Optimum viscoelastic absorbers for cubic nonlinear systems," *J. Vibrat. Control*, vol. 20, no. 10, pp. 1464–1474, Jul. 2014, doi: 10.1177/1077546312473322.

[8] F. Beltrán-Carbajal and G. Silva-Navarro, "Active vibration control in duffing mechanical systems using dynamic vibration absorbers," *J. Sound Vibrat.*, vol. 333, no. 14, pp. 3019–3030, Jul. 2014, doi: 10.1016/j.jsv.2014.03.002.

[9] J. C. Ji, "Secondary resonances of a quadratic nonlinear oscillator following two-to-one resonant Hopf bifurcations," *Nonlinear Dyn.*, vol. 78, no. 3, pp. 2161–2184, Nov. 2014, doi: 10.1007/s11071-014-1588-6.

[10] J. Yang, Y. P. Xiong, and J. T. Xing, "Power flow behaviour and dynamic performance of a nonlinear vibration absorber coupled to a nonlinear oscillator," *Nonlinear Dyn.*, vol. 80, no. 3, pp. 1063–1079, May 2015, doi: 10.1007/s11071-014-1556-1.

[11] J. C. Ji, "Two families of super-harmonic resonances in a time-delayed nonlinear oscillator," *J. Sound Vibrat.*, vol. 349, pp. 299–314, Aug. 2015, doi: 10.1016/j.jsv.2015.03.049.

[12] X. Sun and X. Jing, "Multi-direction vibration isolation with quasi-zero stiffness by employing geometrical nonlinearity," *Mech. Syst. Signal Process.*, vols. 62–63, pp. 149–163, Oct. 2015, doi: 10.1016/j.ymssp.2015.01.026.

[13] M. Febbo, E. M. Lopes, and C. Bavastri, "Influence of temperature on optimum viscoelastic absorbers in cubic nonlinear systems," *J. Vibrat. Control*, vol. 22, no. 15, pp. 3396–3412, Aug. 2016, doi: 10.1177/1077546314560202.

[14] N. Han and Q. Cao, "Global bifurcations of a rotating pendulum with irrational nonlinearity," *Commun. Nonlinear Sci. Numer. Simul.*, vol. 36, pp. 431–445, Jul. 2016, doi: 10.1016/j.cnsns.2015.12.009.

[15] W. A. El-Ganaini, A. Kandil, M. Eissa, and M. Kamel, "Effects of delayed time active controller on the vibration of a nonlinear magnetic levitation system to multi excitations," *J. Vibrat. Control*, vol. 22, no. 5, pp. 1257–1275, Mar. 2016, doi: 10.1177/1077546314536753.

[16] Y. Shen, L. Chen, X. Yang, D. Shi, and J. Yang, "Improved design of dynamic vibration absorber by using the inerter and its application in vehicle suspension," *J. Sound Vibrat.*, vol. 361, pp. 148–158, Jan. 2016, doi: 10.1016/j.jsv.2015.06.045.

[17] X. Sun and X. Jing, "A nonlinear vibration isolator achieving high-static-low-dynamic stiffness and tunable anti-resonance frequency band," *Mech. Syst. Signal Process.*, vol. 80, pp. 166–188, Dec. 2016, doi: 10.1016/j.ymssp.2016.04.011.

[18] N. Han and Q. Cao, "Rotating pendulum with smooth and discontinuous dynamics," *Int. J. Mech. Sci.*, vol. 127, pp. 91–102, Jul. 2017, doi: 10.1016/j.ijmecsci.2016.09.024.

[19] J. C. Ji and T. Brown, "Periodic and chaotic motion of a time-delayed nonlinear system under two coexisting families of additive resonances," *Int. J. Bifurcation Chaos*, vol. 27, no. 5, May 2017, Art. no. 1750066, doi: 10.1142/S0218127417500663.

[20] A. Kandil and W. A. El-Ganaini, "Investigation of the time delay effect on the control of rotating blade vibrations," *Eur. J. Mech. A/Solids*, vol. 72, pp. 16–40, Nov. 2018, doi: 10.1016/j.euromechsol.2018.03.007.

[21] D. Lavazec, G. Cumunel, D. Duhamel, and C. Soize, "Experimental evaluation and model of a nonlinear absorber for vibration attenuation," *Commun. Nonlinear Sci. Numer. Simul.*, vol. 69, pp. 386–397, Apr. 2019, doi: 10.1016/j.cnsns.2018.10.009.

[22] C.-X. Liu, Y. Yan, and W.-Q. Wang, "Primary and secondary resonance analyses of a cantilever beam carrying an intermediate lumped mass with time-delay feedback," *Nonlinear Dyn.*, vol. 97, pp. 1175–1195, Jul. 2019, doi: 10.1007/s11071-019-05039-w.

[23] Y. Wang, X. Jing, H. Dai, and F.-M. Li, "Subharmonics and ultra-subharmonics of a bio-inspired nonlinear isolation system," *Int. J. Mech. Sci.*, vol. 152, pp. 167–184, Mar. 2019, doi: 10.1016/j.ijmecsci.2018.12.054.

[24] J. Awrejcewicz, A. Cheaib, N. Losyeva, and V. Puzyrov, "Responses of a two degrees-of-freedom system with uncertain parameters in the vicinity of resonance 1:1," *Nonlinear Dyn.*, vol. 101, no. 1, pp. 85–106, Jul. 2020, doi: 10.1007/s11071-020-05710-7.

[25] Y. S. Hamed, A. Kandil, and J. T. Machado, "Utilizing macro fiber composite to control rotating blade vibrations," *Symmetry*, vol. 12, pp. 1–23, Dec. 2020, doi: 10.3390/sym12121984.

[26] Y. S. Hamed and A. Kandil, "Influence of time delay on controlling the non-linear oscillations of a rotating blade," *Symmetry*, vol. 13, pp. 1–18, Jan. 2021, doi: 10.3390/sym13010085.

[27] C.-X. Liu, Y. Yan, and W.-Q. Wang, "Resonance and chaos of micro and nano electro mechanical resonators with time delay feedback," *Appl. Math. Model.*, vol. 79, pp. 469–489, Mar. 2020, doi: 10.1016/j.apm.2019.10.047.

[28] S. Salighe and H. Mohammadi, "MIMO adaptive control for suppression the vibrations of a nonlinear interconnected structure with abrupt changes in the excitation loads," *ISA Trans.*, vol. 98, pp. 123–136, Mar. 2020, doi: 10.1016/j.isatra.2019.08.051.

[29] A. Kandil and Y. S. Hamed, "Tuned positive position feedback control of an active magnetic bearings system with 16-poles and constant stiffness," *IEEE Access*, vol. 9, pp. 73857–73872, 2021, doi: 10.1109/ACCESS.2021.3080457.

[30] A. Kandil, Y. S. Hamed, and A. M. Alsharif, "Rotor active magnetic bearings system control via a tuned nonlinear saturation oscillator," *IEEE Access*, vol. 9, pp. 133694–133709, 2021, doi: 10.1109/ACCESS.2021.3114356.

[31] C. Liu, Y. Yan, and W.-Q. Wang, "Optimal delayed control of primary and second resonances of an electrostatic driving double-sided micro-actuator," *Chaos, Solitons Fractals*, vol. 142, Jan. 2021, Art. no. 110499, doi: 10.1016/j.chaos.2020.110499.

[32] S. Mohanty and S. K. Dwivedy, "Linear and nonlinear analysis of traditional and non-traditional piezoelectric vibration absorber with time delay feedback for simultaneous resonance conditions," *Mech. Syst. Signal Process.*, vol. 161, Dec. 2021, Art. no. 107980, doi: 10.1016/j.ymssp.2021.107980.
[33] Y. Yan, J. Xu, M. Wiercigroch, and Q. Guo, "Statistical basin of attraction in time-delayed cutting dynamics: Modelling and computation," *Phys. D, Nonlinear Phenomena*, vol. 416, Feb. 2021, Art. no. 132779, doi: 10.1016/j.physd.2020.132779.
[34] J. Zhou, W. Zhang, X. S. Wang, B. P. Mann, and E. H. Dowell, "Primary resonance suppression of a base excited oscillator using a spatially constrained system: Theory and experiment," *J. Sound Vibrat.*, vol. 496, Mar. 2021, Art. no. 115928, doi: 10.1016/j.jsv.2020.115928.
[35] D. Ma, X. Cao, C. Sun, R. Wang, Q. Sun, X. Xie, and P. Wang, "Dual-predictive control with adaptive error correction strategy for AC microgrids," *IEEE Trans. Power Del.*, early access, Aug. 2, 2021, doi: 10.1109/TPWRD.2021.3101198.
[36] D. Ma, M. Liu, H. Zhang, R. Wang, and X. Xie, "Accurate power sharing and voltage regulation for AC microgrids: An event-triggered coordinated control approach," *IEEE Trans. Cybern.*, pp. 1–11, 2021, doi: 10.1109/TCYB.2021.3095959.
[37] A. H. Nayfeh, *Introduction to Perturbation Techniques*. New York, NY, USA: Wiley, 1993.
[38] A. H. Nayfeh and B. Balachandran, *Applied Nonlinear Dynamics*. New York, NY, USA: Wiley, 1995.

ALI KANDIL received the M.Sc. and Ph.D. degrees in vibration control of nonlinear dynamical systems from the Faculty of Electronic Engineering, Menoufia University, in 2014 and 2018, respectively. He is currently working with the Faculty of Electronic Engineering, Menoufia University, as an Assistant Professor of engineering mathematics. His current research interests include vibration control, nonlinear dynamics, bifurcation theory, and stability theory.

Y. S. HAMED received the M.Sc. and Ph.D. degrees in mathematics from the Faculty of Science, Menoufia University, Egypt, in 2005 and 2009, respectively. He is currently a Professor of engineering mathematics with the Department of Physics and Engineering Mathematics, Faculty of Electronic Engineering, Menoufia University. He has been a Professor of mathematics with the Department of Mathematics and Statistics, Taif University, Saudi Arabia. He supervised and examined some of the M.Sc. and Ph.D. candidates. His research interests include theory of differential equations and its application, numerical analysis, modeling, dynamical systems control, chaotic systems, renewable energy systems, vibration control and computational methods for solving differential equations, and engineering systems. He is also an Editor of the *International Journal of Control, Automation and Systems* (IJCAS).

ABDULLAH M. ALSHARIF received the Ph.D. degree in mathematics for engineering science from the University of Birmingham, U.K. He has published research articles in reputed international journals of mathematical and engineering sciences. His research interests include applied mathematics and mathematical physics, including the mathematical methods and models for complex systems, Newtonian and non-Newtonian fluids, mathematical engineering, and numerical methods for rheological fluids. He is a referee of mathematical journals.

JAN AWREJCEWICZ is currently the Head of the Department of Automation, Biomechanics and Mechatronics, Lodz University of Technology, where he has been the Head of the Ph.D. School on Mechanics, since 1996, and the Head of graduate/postgraduate programs on mechatronics, since 2006. He has been a Corresponding Member of the Polish Academy of Sciences, since 2016. He has authored/coauthored over 830 journal articles and refereed international conference papers and 53 monographs. His papers and research cover various disciplines of mechanics, material science, biomechanics, applied mathematics, automation, physics, and computer-oriented sciences, with main focus on nonlinear processes. He was a recipient of the Doctor Honoris Causa (Honorary Professor) of the Academy of Arts and Technology, Bielsko-Biala, Poland, in 2014; the Czestochowa University of Technology, Czestochowa, Poland, in 2014; the Kielce University of Technology, in 2019; the National Technical University "Kharkiv Polytechnic Institute," in 2019; and the Gdańsk University of Technology in 2019. He was also a recipient of numerous honors and awards, including the prestigious Alexander von Humboldt Award (twice). He is also the editor-in-chief of three international journals, a member of the Editorial Board of 90 international journals (23 with IF), and an editor of 33 books and 37 journal special issues. For more information please visit www.abm.p.lodz.pl.